

**The Role of Transport Phenomena in Whispering Gallery Mode
Optical Biosensor Performance**

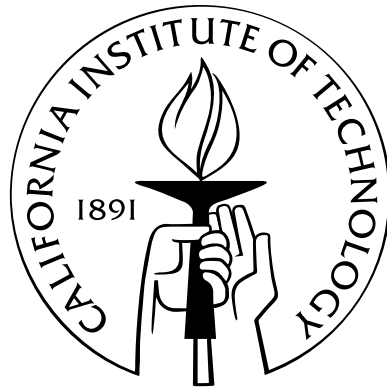
Thesis by

Jason Gamba

In Partial Fulfillment of the Requirements

for the Degree of

Doctor of Philosophy



California Institute of Technology

Pasadena, California

2012

(Defended June 3, 2011)

© 2012

Jason Gamba

All Rights Reserved

For Ashley, my wife and friend. Everything changed when I met you.

Acknowledgements

The fact that a single name appears on the title page of a dissertation can be quite misleading. Neither this document, nor the research behind it, could have been completed without the help of a great number of people.

I would first like to thank my advisor, Professor Rick Flagan, who has given me the opportunity to work on a project I truly enjoy. I came to him at the end of my third year of graduate school seeking help from the Executive Officer of Chemical Engineering with finding a new research home on campus. I was looking for a project in a research lab that could support me while I completely rebooted my graduate career, and hoped Professor Flagan could advise me on how to go about my search. After listening to me describe my situation for nearly an hour, he politely asked if I would be interested in hearing about a project available in his own group involving an extraordinary optical biosensor. Within days I was a Flagan Lab member, eager to return to my roots as a chemical engineer by applying the field's core disciplines to the analysis of what was essentially a physicist's toy. Professor Flagan has taught me a great deal about instrument development and validation, and working in his lab has been an excellent education as a researcher.

I am also very grateful to Professor Andrea Armani, who has been a valuable mentor and friend to me since we began working together in 2008. It was her work as a Clare Boothe Luce Postdoctoral Fellow that began the collaboration between the Flagan, Vahala, and Fraser laboratories at Caltech, of which I have been a part. I was fortunate enough to learn this field from her, and benefit from the extraordinary care and patience she put into developing the procedures she used for her experiments. Even after Professor Armani accepted her faculty position at the University of Southern California, she continued to offer her time to answer my (seemingly endless) questions. I cannot express how helpful this was for a researcher trying to

learn a field outside his expertise. Working with her and getting to know her has truly been one of the most rewarding pieces of my graduate career.

I would like to thank Professors Scott Fraser and Mark Davis as well for all of their helpful suggestions and guidance as members of my thesis committee. Of course, my work would not have been possible at all if not for the much-appreciated funding from the Jacobs Institute for Molecular Engineering for Medicine at the California Institute of Technology.

I have also been fortunate to work alongside a wonderful group of researchers in the Flagan/Seinfeld Laboratory. The person who has most affected my own research is Xerxes Lopez-Yglesias. He is a resource of incalculable value to the group, with nearly everyone relying on his broad expertise at one point or another during their tenure. He and I conducted a thorough analysis of the physics involved in sensing a single biomolecule with a whispering gallery mode sensor, debating the value of previous methods and the interpretation of reference texts for hours on end. This intense academic endeavor led us to two main conclusions: (i) that theoretical modeling comes entirely down to how you justify the shortcuts you took in order to preserve your sanity, and (ii) that the selection of Pasadena dining establishments open at 3 am is sadly limited.

Andy Downard is another fine groupmate to whom I am indebted. In addition to being a good friend, Andy was of particular help with my efforts to model the fluid flow around sensors. He contributed even more to the daily operations of the lab by generously providing organizational advice and encouraging a multidisciplinary spirit that is too often absent in research environments. Our research group often posed unique challenges, as everyone must quickly develop a broad range of abilities in order to make any progress. I am grateful, however, to *all* the members of the Flagan and Seinfeld groups for creating a cooperative and friendly atmosphere, which should never be taken for granted. You all conduct your research (and yourselves) with class in the face of overwhelming pressure to succeed at any cost.

I would also like to thank two outstanding collaborators, Jacob Sendowksi and Naresh Satyan, for their friendship, help, and patience during our work to integrate a tunable laser source of their creation into the nascent sensor apparatus described in the chapters that follow here. Along with the help of other members

of the Yariv Laboratory in Applied Physics and Electrical Engineering, especially Scott Steger and Arseny Vasilyev, we began what I hope is a long and productive research partnership for our groups. From the many, many hours I spent working with Jacob and Naresh, I can say that both represent the finest that Caltech has to offer. They are excellent scientists and just truly fun people to be around, both of which only made the grueling frustration of troubleshooting a relatively untested experimental setup that much more pleasant.

Though they get too little credit for the impact they have on student life and graduate research, the various staff at Caltech also deserve a great deal of gratitude. Chemical Engineering administrative assistants like Kathy Bubash, Laura King, Anne Hormann, Marcy Fowler, Martha Hepworth, Karen Baumgartner, and Yvette Grant play a huge role in making sure students have access to their advisors and that the academic machinery continues to run smoothly for everyone. Additionally, a great systems administrator like Suresh Gupta is pivotal in a research environment like Caltech where computation and data storage/transfer are so important. Technical staff, including machinists like Mike Roy, Steve Olsen, and Mike Vondrus as well as glassblowers like Rick Gerhart, are also valuable resources that allow students to push the envelope of their field by creating new equipment and techniques. It also helps that they are all so friendly, welcoming, and generous with their time. I would like to thank all of these fine Caltech staff members for all of the tasks, large and small, they have helped me with since I started here. I would especially like to thank Mike Roy for teaching me so much about machining and for being such a great friend to me through all of my frustrations. He is a bright and inquisitive man who perfectly embodies the spirit of Caltech's ingenuity and curiosity.

I also want to point out the contributions that another staff member, Dr. Mike Vicic, has made to my graduate career. He is a truly gifted educator who cares deeply about helping his students learn *and remember* as much of the mountain of information that the Chemical Engineering curriculum presents to them as possible. I TAed courses administered by Mike three times, and I may have learned more TAing his undergraduate courses than I did during my own undergraduate career. I want to thank him for all of the conversations and guidance he has given me as my friend and unofficial mentor. I cannot overstate his value to the Chemistry and Chemical Engineering Division, or to the many students that get the chance to

interact with him.

One of the most important reasons I chose to come to Caltech for graduate school was the altogether wonderful people that I would get to study with in Chemical Engineering. Though the majority of them graduated (well) before me, I consider myself fortunate to have worked with such a fine group as them. I am truly lucky to have met and learned from people like Brendan Mack, Nick Brunelli, Yoshie Narui, Chris Alabi, Jim Van Deventer, Chase Beisel, and John McKeen. Thank you all for making Caltech such a wonderful place to be and learn.

These and many other friends enriched my life and helped me make it through the more difficult times in graduate school. Matt Jacob-Mitos and I left Rensselaer Polytechnic Institute as best friends, which is probably why he followed me out to the West Coast for school (albeit to a different university). I shudder to put this in writing lest he never let me live it down, but he is one of the brightest people I have ever met and he makes things fun. I owe him a great deal for supporting and continually encouraging my pursuit of a Ph.D. Additionally, Charlotte Mack has been a constant source of fun since I met her many years ago. She is a voice of comfort and inspiration, and her love of life and learning is contagious. I am so very grateful to her and her husband, Brendan, for all of their support through graduate school, my ongoing job search, and life in general. Other brilliant and wonderful friends like Sara Broadhead, Rick Tabor, Chris and Jessica Hansen, and Jackie Kopcsak have all helped me keep a healthy perspective by letting me think and talk about something other than science during all of the fun times we have gotten to spend together. To all of these great friends I give my love, admiration, and thanks.

I want to thank my wonderful family for their extraordinary support. My parents, David and Eileen, have always fostered my curiosity and joy for learning, but their love and encouragement has meant a great deal to me. They have worked so hard to make sure every possible educational opportunity was available to their children, from pre-kindergarten to this day. They have always given me the freedom to pursue my interests, even when that carried me 3000 miles away for graduate school. I am truly fortunate to have such caring and giving parents. I could not have accomplished any of this without their sacrifice and love. I want to thank them for all of this, and for raising me a Red Sox fan.

My entire family has helped me get to this point in my life. I want to thank, in particular, all of my grandparents for being such wonderful examples of how people should treat each other and approach their lives and their work. They are and were passionate individuals, and I love them very much.

Thank you, also, to my brother, David, for always backing me up and helping me to persevere through his encouragement and love. You are the best big brother and friend anybody could have.

Finally, I want to thank my wonderful wife, Ashley. Everything in my life improved when I met you. There is no way I can thank you enough for the sacrifices you have made or the lengths to which you have gone to help me on this (regrettably) long road to graduation. You are an extraordinary woman who volunteered to live the lavish life of a graduate student's wife. I still do not understand what saintly feat I must have accomplished to deserve you, but I am grateful everyday because chance sat me next to you on that airplane. Thank you so very much.

Abstract

Whispering gallery mode (WGM) optical resonator sensors have emerged as promising tools for label-free detection of biomolecules in solution. These devices have even demonstrated single-molecule limits of detection in complex biological fluids. This extraordinary sensitivity makes them ideal for low-concentration analytical and diagnostic measurements, but a great deal of work must be done toward understanding and optimizing their performance before they are capable of reliable quantitative measurements. The present work explores the physical processes behind this extreme sensitivity and how to best take advantage of them for practical applications of this technology.

I begin by examining the nature of the interaction between the intense electromagnetic fields that build up in the optical biosensor and the biomolecules that bind to its surface. This work addresses the need for a coherent and thorough physical model that can be used to predict sensor behavior for a range of experimental parameters. While this knowledge will prove critical for the development of this technology, it has also shone a light on nonlinear thermo-optical and optical phenomena that these devices are uniquely suited to probing.

The surprisingly rapid transient response of toroidal WGM biosensors despite sub-femtomolar analyte concentrations is also addressed. The development of asymmetric boundary layers around these devices under flow is revealed to enhance the capture rate of proteins from solution compared to the spherical sensors used previously. These lessons will guide the design of flow systems to minimize measurement time and consumption of precious sample, a key factor in any medically relevant assay.

Finally, experimental results suggesting that WGM biosensors could be used to improve the quantitative detection of small-molecule biomarkers in exhaled breath condensate demonstrate how their exceptional sensitivity and transient response can enable the use of this noninvasive method to probe respiratory distress.

WGM bioensors are unlike any other analytical tool, and the work presented here focuses on answering engineering questions surrounding their performance and potential.

Contents

Acknowledgements	iv
Abstract	ix
List of Figures	xiv
List of Tables	xxiii
1 Introduction	1
1.1 History and Context	1
1.2 Thesis Structure	3
2 Biosensors	5
2.1 Overview	5
2.2 Specific Detection	6
2.3 Sample Delivery Methods	14
2.4 Biosensor Performance Metrics	15
2.5 Biosensor Technologies	17
3 Whispering Gallery Mode Resonators as Biosensors	27
3.1 Resonance	28
3.2 WGM Mode Structure	30
3.3 Quality Factor	32

3.4	WGM Resonator Fabrication	37
3.5	Coupling Light into WGM Resonators	42
3.6	Nonlinear Effects in WGM Resonators	46
3.7	Sensing with WGM Resonators	48
4	Flow-Enhanced Transient Response in Whispering Gallery Mode Biosensors	53
4.1	Abstract	53
4.2	Introduction	53
4.3	Boundary Layers	54
4.4	Supplemental Information	61
5	The Physics of Extreme Sensitivity in WGM Optical Resonator Biosensors	68
5.1	Abstract	68
5.2	Introduction	69
5.3	The WGM Biosensing Experiment	70
5.4	Existing Models of WGM Biosensor Behavior	74
5.5	Physical Processes in WGM Sensing	77
5.6	Modeling WGM Biosensors	88
5.7	Results and Discussion	90
5.8	Conclusions	93
5.9	Supplemental Information	94
6	Detection of Biomarkers for Respiratory Distress in Exhaled Breath Condensate	99
6.1	Biomarkers for Oxidative Stress	100
6.2	Whispering Gallery Mode Optical Biosensors	102
6.3	Detection of Model Biomarkers	103
7	Conclusions and Future Work	112

7.1	Summary	112
7.2	Future Work	114
Bibliography		130

List of Figures

2.1	An equilibrium binding curve for Interleukin-2 with its T Lymphocyte receptor according to Eq. (2.6). Note the sigmoidal shape whose slope approaches zero in the limit of both high and low analyte concentrations. At low $[A]$, the large relative changes in concentration are still too small in terms of total analyte molecules bound. In contrast, the sensor surface is saturated at high $[A]$ and changes in concentration make little affect little change in sensor signal. K_D is marked at 6.5×10^{-10} M.	9
2.2	This antibody features four polypeptides: two heavy chain (red) and two light chain (blue). Note also the "stem-and-arms" configuration, with one F_C and two F_{AB} regions. The two complementarity-determining regions (CDRs), where analyte binding occurs, are noted at the end of the two F_{AB} regions.	11
2.3	The non-covalent functionalization of a biosensor surface via the non-specific adsorption of Protein G (green) and antibody (black). Exposure to analyte (blue) will lead to binding according to the equilibrium expression in Eqs. (2.1)–(2.4). Note the random orientation of the Protein G molecules as well as the fact that not all such molecules are occupied by an antibody.	13

2.4	Methods for delivering sample to a biosensor. (a) The simple batch method, wherein a droplet of solution is placed onto a planar sensor and diffusion delivers sample to the device surface. (b) The open flow cell with flow injection, featuring a substrate and glass coverslip to form the top and bottom. Surface tension prevents the water from draining, requiring that either the top and bottom surfaces be sufficiently wettable <i>or</i> the gap sufficiently small. (c) The microfluidic flow cell, a subset of the closed flow cells. These devices are typically made using soft lithography techniques, and their microscale features ensure laminar flow and very little mixing.	15
2.5	Field effect transistors (FETs). (a) A generic FET, including the source and drain with conduction channel between the two. A field applied using the gate can control the density of charge carriers in the conduction channel and change the current measured at the drain. (b) A nanowire field effect transistor (FET) sensor. Biomolecules bound to the surface of the nanowire have a localized electric field that can distort the charge carrier density in the nanowire. Changes in the drain current are used to track how much material has adsorbed to the device.	19
2.6	Fluorescence-based biosensor technologies. (a) Total internal reflection fluorescence (TIRF) is characterized by the excitation of fluorescentlytagged species at a surface by an evanescent field that decays exponentially and excites only those fluorophores near the surface. (b) Sandwich assays feature exposure of an antibody-labeled surface to an analyte solution, followed by exposure to a fluorescentlylabeled antibody that binds exclusively to the complex.	24
2.7	Surface plasmon resonance (SPR). Here a surface-propagating wave is generated via total internal reflection in a thin gold film deposited on silica in order to excite a surface plasmon in the metal. Material that adsorbs to the surface shifts the plasmon resonance, which must be compensated for by altering the incident angle of light or the incident wavelength. In this way the surface binding reaction between immobilized targeting species and analyte may be monitored.	26
3.1	Whispering gallery mode resonance in the limit of geometric optics.	28

3.2	(a) A toroidal WGM resonator with a cut plane marked in green. (b) An image of the normalized mode intensity along the cut plane in (a) as calculated using the finite element solver COMSOL Multiphysics. (c) A closer look at the normalized mode structure along the cut line in (b) shows the evanescent field that extends into the water.	31
3.3	Flowing PBS buffer into the flow cell changes the refractive index of the surrounding medium, thereby causing a resonance shift according to Eq. (3.10). This is a basic and non-specific sensing method.	33
3.4	Transmission spectra depicting a resonance red-shifting a distance $\Delta\lambda$ in wavelength-space in response to adsorption of protein to the resonator surface. The minimum fractional transmission, along with the total transmission when no light is coupled into the resonator, may be used to calculate the coupled power P_D . The value of Q may also be determined using the observed value of $\delta\lambda_R$ and Eq. (3.12).	34
3.5	The four-step process to fabricate toroidal WGM resonators on (a) a bare silicon wafer with 2 μm of thermal oxide. (b) Photolithography is used to define a pattern of silica discs through a buffered oxide etch process. (c) The chip is exposed to XeF_2 , a gas that isotropically and selectively etches the silicon from beneath the silica disks. (d) A CO_2 laser at 10.6 μm wavelength light is focused normal to the microdisks, melting the edges and leaving microtoroid resonators on silicon pedestals.	39
3.6	Three photographs of a single disk during an experiment to use a a KOH etch procedure (10 minute piranha clean followed by a 90 minute exposure to 30 wt% KOH in water) to define a silica disk followed by reflow with a CO_2 laser. The anisotropic nature of the KOH etch produces an off-round pedestal, eliminating any chance of a smooth toroid. Note: field of view in all images is 310 μm wide	40

3.7	Diagrams of experimental reflow apparatus. The black arrow indicates the laser source. Plano-convex (PC) lenses made from ZnSe, which does not absorb light at $10.6 \mu\text{m}$ like silica optics do, are also shown. The alternative setup proposed in (b) may have the advantages of a cleaner beam profile due to both the spatial filter (pinhole) as well as better control over the beam diameter entering the third PC lens.	41
3.8	Coupling of 633 nm light into a $125 \mu\text{m}$ diameter optical fiber in water with $Q = 2.3 \times 10^7$. .	43
3.9	Coupling 633 nm light into a microcylindrical WGM resonator. (a) Illumination of the taper and resonator by a bright field, and (b) illumination of the system by only the coupled light. The bright spots in (b) indicate how light is coupled into "corkscrew" modes, reaching parts of the fiber far from the taper and being scattered.	43
3.10	Typical transmission profiles illustrating the under-coupled, critically-coupled and over-coupled regimes.	45
3.11	Nonlinear effects observed while coupling into WGM resonators. (a) Asymmetrical transmission trough for a $150 \mu\text{m}$ microdisk excited with 1310 nm light. (b) Opto-mechanical oscillations as the momentum of propagating light excites mechanical vibration modes in a microtoroidal resonator excited with 1540 nm light. (c) A split resonance peak as backscattering in the cavity can break the degeneracy of counter propagating modes in a microtoroidal resonator excited with 1310 nm light	47
3.12	The WGM sensing experimental apparatus, featuring a tunable laser, tapered optical fiber wavguide, resonator, detector and data capture/processing computer. A function generator is used to sweep linearly through wavelength space so that a transmission spectrum may be used to locate the center of the resonance peak or determine the Q of the resonance.	50
3.13	The flow cell used in WGM biosensor experiments, shown with a microtoroidal resonator and tapered optical fiber.	51

3.14	Using a tapered optical fiber waveguide to couple light into a toroid. (a) A view showing the two in proximity to one another. (b) A low-quality toroidal WGM resonator ($Q \approx 10^2$) scattering light out of the cavity.	51
4.1	Concentration profiles for mass transfer to a cylinder in cross section under various flow conditions. Red denotes a normalized concentration of 1, and Blue denotes a normalized concentration of 0. (a) Diffusion alone delivers the species to the cylinder isotropically. (b) At low upstream flow velocity, an asymmetric concentration distribution forms, with an extended boundary layer in the wake of the cylinder. (c) At high upstream flow velocity, the boundary layer is thin and the concentration gradient remains asymmetric and is confined to a narrow region around the cylinder.	55
4.2	Upstream boundary layer thickness δ_{95} as a function of inlet flow velocity for spheres of radius $42.5 \mu\text{m}$ (circles) and $2.5 \mu\text{m}$ (squares) with predicted scaling laws at high (blue) and low (red) flow velocity limits. The inset graph depicts how δ_{95} is determined.	57
4.3	Time between binding events, τ , for 1 fM analyte concentration solution introduced to toroidal (circles) and spherical (squares) WGM sensors. (inset) τ recast as a function of sensor Péclet number.	58
4.4	The effect of sphere radius on δ_{95} for varying inlet flow velocities, calculated using the same model as in Fig. 4.2.	59
4.5	Modeled results for τ at a range of concentrations for Interleukin-2 with $U = 10^{-2}$ compared to experimental data published by Armani et al. [1, 2] collected in buffer (circle) and bovine blood serum (triangle).	60
4.6	Flow cell geometry used in COMSOL Multiphysics simulation of flow around a WGM sensor. The near plane is a symmetry plane that bisects the cell and the resonator. The sensors are cut out of the cell, and their surfaces feature no-slip flow and $C_i = 0$ (i.e., instantaneous surface reaction) boundary conditions.	64

4.7	Flow cell boundary conditions used in COMSOL Multiphysics simulations of flow around WGM sensors. (a) Symmetry plane. (b) "No-slip" and "no flux" conditions. (c) Uniform flow inlet velocity $U = U_{inlet}$ and inlet concentration $C_{inlet} = 1 \text{ fM}$. (d) Flow outlet at pressure $p_0 = 101,325 \text{ Pa}$	65
4.8	The relative surface binding rate to a sphere with $R_{sphere} = 42.5 \mu\text{m}$ and $U_{inlet} = 0.01 \text{ m/s}$ as a function of the surface mesh element size ($l_{mesh} = R_{sphere}/N$), calculated with respect to the case $N = 500$ ($l_{mesh} = 85 \text{ nm}$). This quantity converges with increasing N and achieves a relative error of less than 2% for $N > 80$ (see inset for detail).	66
4.9	Solutions for the normalized mode intensity (NMI) of a (a) toroidal and (c) spherical optical whispering gallery mode resonator. The effective sensing area is determined by where the NMI is greater than 10% of the surface maximum as indicated by dotted lines for (b) a toroid and (d) a sphere.	67
5.1	Part of a simulated transmission spectrum that might be observed by measuring the photodetector output using an oscilloscope while the wavelength is swept at $\frac{d\lambda}{dt} = 1.35 \text{ nm s}^{-1}$ across a resonance with $Q = 10^8$. The full wavelength scan is shown in the inset. The lower horizontal axis is in terms of wavelength detuning from λ_R while the upper is in terms of time.	74
5.2	The normalized mode intensity for $\lambda_R \approx 680 \text{ nm}$ in a (a) spherical ($R = 42.5 \mu\text{m}$) and (b) toroidal ($r_a = 40 \mu\text{m}$, $r_i = 2.5 \mu\text{m}$) WGM resonator.	78
5.3	(a) Rigorous and (b) modified computation schemes for calculating the WGM sensor response.	89
5.4	The normalized mode profile in a toroidal resonator with major radius $r_a = 40 \mu\text{m}$ and minor radius $r_i = 2.5 \mu\text{m}$ corresponding to the shown cut line (inset) and the thermal plume resulting from a single-molecule protein heat source exposed to a mode with $Q = 10^8$ and $P_D = 1 \text{ mW}$ resulting in linear absorption by the molecule.	91
5.5	The temperature at the location of the protein (red) and mode peak (blue) as a function of time where the only heating comes from a protein exhibiting linear absorption bound to the surface of the toroidal sensor with $Q = 10^8$, $P_D = 1 \text{ mW}$, and $\frac{d\lambda}{dt} = 1.35 \text{ nm s}^{-1}$	92

5.6	The resonance shift due to a single-molecule protein heat source for toroidal resonators ($r_a = 40 \mu\text{m}$, $r_i = 2.5 \mu\text{m}$) with $P_D = 1 \text{ mW}$ and $\frac{d\lambda}{dt} = 1.35 \text{ nm s}^{-1}$ for varying quality factor. This shift is plotted against a relative time t/τ_{res} to simplify comparison. The maximum signal is plotted as a function of Q in the inset.	92
5.7	The geometry used in COMSOL Multiphysics to solve Eqn. (5.12) for the transient temperature profile resulting from the excitation of a single-molecule heat source located at what is assumed to be a locally planar interface (blue plane) between a toroidal WGM optical resonator and the water surrounding it. The interior lines are boundaries between subdomains created within the geometry to allow for convenient control over local mesh element size, reducing computation time and memory requirements.	95
5.8	Transmission spectrum for a toroid of major radius $r_a = 40 \mu\text{m}$ and minor radius $r_i = 5 \mu\text{m}$ and $Q \approx 10^7$ at wavelength scan rates of (a) $\frac{d\lambda}{dt} = 7.6 \text{ nm/s}$ and (b) -7.6 nm/s . The resonator is submerged in water and is being excited using a 765 nm external cavity tunable laser, with a maximum coupled power of 2.6 mW. The difference in resonance linewidth and transmission minimum is due to thermal distortion of the Lorentzian trough, where λ_R shifts during the scan when light is absorbed and the system warms. Since this warming results in a red shift of λ_R , a positive scan rate leads to an artificially broad line and a negative scan rate yields an artificially narrow line.	98
6.1	The structures of arachidonic acid and two of its derivatives most useful as biomarkers of oxidative stress	101
6.2	Typical frequency scan profile shape for external cavity laser (red) and chirp laser (blue). Note that the ECL has a wider tuning range; however, the OSFL laser has no moving parts so it may attain a far greater range of scan rates.	104
6.3	Typical sensor response for a microtoroid resonator in water at 1310 nm exposed to 50 $\mu\text{L/min}$ flow of water. The dotted line marks the point at which flow was shut off.	107

6.4	Detection of 100 fM Interleukin-2 in buffer using a toroid with $Q=2.0 \times 10^5$, a flow rate of 50 $\mu\text{L}/\text{min}$, and a testing wavelength of 1310 nm. The dotted line marks when flow was shut off, and the endpoint resonance shift is marked as $\Delta\lambda_{SS}$	109
6.5	Detection of 8-isoprostanate in buffer using a toroid with $Q=4.2 \times 10^5$, a flow rate of 50 μL and a testing wavelength of 1310 nm. The data collection was stitched together to illustrate cumulative resonance shift. First Protein G (red) then polyclonal anti-8ip (blue) were allowed to adsorb. Next, six successively more concentrated 8ip solutions were flown into the cell (100 pM, 1 nM, 10 nM, 100 nM, 1 μM , and 10 μM). The inset expands this part of the curve for clarity.	111
6.6	(a) This sample data for 100 μM 8ip appears to saturate before flow is turned off (dotted line), at which point it reaches a new steady state. The endpoint data sought in this measurement is the value of $\Delta\lambda_{SS}$, the true steady state resonance shift. (b) By collecting this endpoint resonance shift and plotting against the concentration of 8ip that elicited that shift, we have a partial dynamic range curve for this system.	111
7.1	Modeling results for stagnation point flow around a cylinder with adsorption of IL-2 to its antibody. Upstream flowrate is 100 $\mu\text{L}/\text{min}$. (a) Dimensionless surface concentration of bound IL-2 at upstream node and downstream nodes as a function of dimensionless time (with respect to characteristic desorption timescale). Flow geometry as depicted in inset, with red lines depicting streamlines and cylinder diameter of 80 μm . (b) Dimensionless surface concentration of bound IL-2 as a function of arc length from the upstream node ($x = 0 \text{ m}$) to the downstream node ($x = 1.26 \times 10^{-4} \text{ m}$). Each curve corresponds to a single point in time.	117
7.2	This graph shows how the WGM biosensor response appeared for detection of a mixture of streptavidin protein and streptavidin-coated polystyrene nanoparticles (radius $a = 25\text{nm}$) with a biotin-functionalized device. This is not actual data. Note the existence of two equilibria: the first (I) where the surface is populated with bound protein and nanoparticles, and the second (II) where the smaller streptavidin has dissociated and been mostly replaced by nanoparticles.	121

7.3 This microfluidic device diagram demonstrates how the laminar flow in such a device may be used to deposit different targeting species (referred to as *Antibody 1* and *Antibody 2*) on different sensors (labeled *1* and *2*) simultaneously. For sufficiently short channels, diffusive mixing between the adjacent flow paths will be limited to the small area indicated. 127

List of Tables

5.1	Single-molecule and Single-particle Detection Using $\Delta\lambda_R$ for WGM Optical Biosensors	71
5.2	Summary of Functional Dependencies of Physical Properties	88
5.3	Experimental Parameters for Modeling WGM Biosensing Experiment	98
5.4	Physical Properties of Silica and Water at 298 K and 680 nm	98
6.1	Local Concentrations of 8-isoprostanate in the Body [3]	101